Chemical Science

EDGE ARTICLE

View Article Online
View Journal | View Issue

Cite this: *Chem. Sci.*, 2014, **5**, 3204

Reductive silylation of a uranyl dibenzoylmethanate complex: an example of controlled uranyl oxo ligand cleavage†

E. A. Pedrick,[a] G. Wu,[a] N. Kaltsoyannis[b] and T. W. Hayton*[a]

Received 4th April 2014
Accepted 22nd May 2014

DOI: 10.1039/c4sc00996g

www.rsc.org/chemicalscience

Reaction of $UO_2(dbm)_2(THF)$ (dbm = *O*C(Ph)CHC(Ph)*O*) with 1 equiv. of R_3SiH (R = Ph, Et), in the presence of $B(C_6F_5)_3$, results in the formation of $U(OB\{C_6F_5\}_3)(OSiR_3)(dbm)_2(THF)$ (R = Ph, **1**; Et, **2**), which were isolated as red-orange crystalline solids in good yields. Interestingly, the addition of 1 equiv. of H(dbm) to **2** results in protonation of the $-OSiEt_3$ ligand and formation of $U(OB\{C_6F_5\}_3)(dbm)_3$ (**4**) in 33% yield, along with formation of $HOSiEt_3$. Furthermore, addition of $HOSiEt_3$ and 1 equiv. of THF to **4**, results in the formation **2**, revealing that this process is reversible. The two-step conversion of $UO_2(dbm)_2(THF)$ to **4** represents a rare example of controlled uranyl oxo ligand cleavage at ambient temperature and pressure. Comparison of diffraction and density functional theory data for **4** suggests the presence of the inverse trans influence, with a very shallow potential energy well for distortion along the trans U–O bond.

Introduction

Reduction of the uranyl moiety (UO_2^{2+}) to U(IV) has proven to be a viable strategy for the treatment of contaminated legacy sites.[1–5] However, reduction to U(IV) requires the disruption of the strong U–O triple bond,[6,7] and as a result, cleavage of the uranyl ion is quite challenging.[8] A variety of strategies have been established over the past 20 years to effect functionalization and cleavage of uranyl, including the use of strongly electron donating equatorial co-ligands,[9] the deployment of strong electrophiles,[10–12] and reductive silylation.[8] Amongst these transformations, reductive silylation has proven to be the most successful and features the greatest scope.[13–19] Reductive silylation was first demonstrated by Arnold and co-workers, who showed that a strongly donating macrocyclic ligand promoted the reductive silylation of $UO_2(THF)(H_2L)$ (L = 'Pacman' polypyrrolic macrocycle) to produce the U(V) silyloxide, $[UO(OSiMe_3)(THF)Fe_2I_2L]$.[13,14,20,21] Subsequently, our research group reported the reductive silylation of the β-ketoiminate complex, $UO_2(^{Ar}acnac)_2$ ($^{Ar}acnac$ = Ar*N*C(Ph)CHC(Ph)*O*; Ar = 3,5-$^tBu_2C_6H_3$) using a combination of $B(C_6F_5)_3$ and $HSiR_3$ (R = Ph, Et) to generate $U(OSiPh_3)(OB\{C_6F_5\}_3)(^{Ar}acnac)_2$[22] and $[U(OSiEt_3)_2(^{Ar}acnac)_2][HB(C_6F_5)_3]$.[23] In our original report we argued that the strong electron donating ability of the β-ketoiminate ligand, $^{Ar}acnac$,[22] activated the uranyl oxo groups toward functionalization. Other researchers have also hypothesized that strongly donating equatorial groups weaken the U=O bond and activate the oxo ligands toward functionalization and/or substitution.[24–27] This hypothesis is supported by vibrational data, which shows a clear correlation between donor ability and the U=O ν_{sym} stretch.[8] Other methods of reductive functionalization of the uranyl ion have also been reported, including reductive lithiation,[28] reduction and functionalization with lanthanide amides,[29,30] and oxo ligand metalation.[31–35]

While actinide chemists now have several procedures in place for functionalizing the uranyl oxo ligand, there are only a few examples of complete uranyl oxo bond cleavage. For example, Ephritikhine and co-workers demonstrated that addition of excess Me_3SiX (X = Cl, Br, I) to $UO_2I_2(THF)_3$ in MeCN resulted in formation of $UX_4(MeCN)_4$ in good yields.[36] In this case, the oxo ligands of the uranyl fragment are thought to be converted into $Me_3SiOSiMe_3$. In another example, the reaction of $[Ph_4P]_2[UO_2Cl_4]$ with thionyl chloride generated the U(VI) mono-oxo, $[Ph_4P][UOCl_5]$.[12] While this synthesis results in U=O bond cleavage at ambient conditions, the mechanism by which this reaction proceeds, and the fate of the missing oxo ligand, are not certain. More recently, Gibson and co-workers demonstrated that the uranyl complex, $[UO_2(NCO)Cl_2]^-$, converts into a terminal nitrido complex, $[NUOCl_2]^-$, and CO_2 in the gas phase *via* collision induced dissociation (CID).[37]

Herein, we report a new example of reductive silylation, using $B(C_6F_5)_3$-activated silane to functionalize the oxo ligands of a dibenzoylmethanate-supported uranyl complex. In addition, we demonstrate a two-step procedure for the controlled cleavage of a uranyl oxo ligand under ambient conditions.

[a]*Department of Chemistry and Biochemistry, University of California Santa Barbara, Santa Barbara, CA 93106, USA. E-mail: hayton@chem.ucsb.edu*

[b]*Christopher Ingold Laboratories, Department of Chemistry, University College London, 20 Gordon Street, London WC1H 0AJ, UK*

† Electronic supplementary information (ESI) available: Crystallographic details and spectral data for **1–4**; optimized Cartesian coordinates for **4** and $[UOCl_5]^-$. CCDC 994968–994971. For ESI and crystallographic data in CIF or other electronic format see DOI: 10.1039/c4sc00996g

Notably, $B(C_6F_5)_3$-activated silanes have been shown to reduce a variety of organic substrates, including ketones, enols and imines.[38–43]

Results and discussion

To expand the scope of borane-mediated silylation of uranyl, the utility of dibenzoylmethanate, dbm (dbm = *O*C(Ph)CHC(Ph)*O*), as a uranyl supporting ligand was probed. Several $UO_2(dbm)_2(L)$-type complexes have been reported in the literature, however they typically feature Lewis base co-ligands that could be incompatible with our reductive silylation protocol (*e.g.*, H_2O, dmso, dmf).[44–46] Thus, we endeavoured to synthesize a uranyl dibenzoylmethanate complex that contained THF as a co-ligand. Reaction of 2 equiv. of Na(dbm), generated *in situ*, with $UO_2Cl_2(THF)_3$ results in formation of a light orange solution, from which $UO_2(dbm)_2(THF)$ can be isolated as an orange powder in 71% yield. This complex features a singlet at 7.32 ppm in its ^1H NMR spectrum (CD_2Cl_2), which is assignable to the γ-CH of the dbm ligand. In addition, broad singlets at 4.99 and 2.47 ppm, confirm the presence of THF in the uranyl coordination sphere. $UO_2(dbm)_2(THF)$ had been reported previously,[47] but had not been fully characterized. It is closely related to several other uranyl bis(β-diketonate) complexes that have been reported in the literature,[46,48] including $UO_2(acac)_2(THF)$,[49] $UO_2(dbm)_2(dmso)$,[45] and $UO_2(dbm)_2(H_2O)$.[44]

With $UO_2(dbm)_2(THF)$ in hand we evaluated the strength of its U=O bonds relative to the previously characterized β-ketoiminate complex, $UO_2(^{Ar}acnac)_2$. A cyclic voltammogram of $UO_2(dbm)_2(THF)$ in CH_2Cl_2 reveals an irreversible reduction feature at $E = -1.19$ V (*vs.* Fc/Fc^+), measured at a scan rate of 0.1 V s^{-1}, which we attribute to the UO_2^{2+}/UO_2^{+} redox couple (Fig. S1†). This feature is irreversible at all scan rates. Importantly, this value is less negative than that observed for $UO_2(^{Ar}acnac)_2$ ($E_{1/2} = -1.35$ V *vs.* Fc/Fc^+),[50] confirming that the dbm equatorial ligand is less electron donating than the $^{Ar}acnac$ ligand, and suggesting a lesser degree of oxo ligand activation in $UO_2(dbm)_2(THF)$. For further comparison, $UO_2(dbm)_2(dmso)$ features a reversible UO_2^{2+}/UO_2^{+} redox couple at $E_{1/2} = -1.36$ V (*vs.* Fc/Fc^+, in dmso),[45] while $UO_2(dbm)_2(dmf)$ features a reversible UO_2^{2+}/UO_2^{+} redox couple at $E_{1/2} = -1.46$ V (*vs.* Fc/Fc^+, in dmf).[46] These lower redox potentials undoubtedly reflect the strong donating ability of dmso and dmf *vs.* THF. In addition, $UO_2(dbm)_2(THF)$ features a U=O ν_{sym} mode of 823 cm^{-1} in its Raman spectrum (Fig. S2†). For comparison, the U=O ν_{sym} mode for $UO_2(^{Ar}acnac)_2$ was determined to be 812 cm^{-1},[51] which reveals that the U=O bonds in $UO_2(dbm)_2(THF)$ are stronger than those in $UO_2(^{Ar}acnac)_2$, and further supports the claim that the dbm ligand is less electron donating. This latter point is a critical because it will allow us to evaluate the effect of a weaker donating equatorial ligand on both reduction and functionalization. Previously, we hypothesized that only strong donor ligands, such as $^{Ar}acnac$, were able to activate uranyl toward functionalization.[51]

Upon establishing that dbm was a weaker donor than $^{Ar}acnac$, we subjected $UO_2(dbm)_2(THF)$ to our reductive silylation protocol. Thus, addition of 1 equiv. of $HSiPh_3$ to $UO_2(dbm)_2(THF)$, in the presence of 1 equiv. of $B(C_6F_5)_3$, results in the formation of a deep red solution, from which U(OB{C_6F_5}$_3$)(OSiPh$_3$)(dbm)$_2$(THF) (**1**) can be isolated as a dark red crystalline material in 62% yield (eqn (1)). Similarly, addition of 1 equiv. of $HSiEt_3$ to $UO_2(dbm)_2THF$, in the presence of 1 equiv. of $B(C_6F_5)_3$, results in the formation of U(OB{C_6F_5}$_3$)(OSiEt$_3$)(dbm)$_2$(THF) (**2**), which can be isolated in 55% yield (eqn (1)). Isolation of both **1** and **2** proceed with higher yield if 0.25 equiv. of THF is added to the mother liquor. The reductive silylation of $UO_2(dbm)_2(THF)$ is similar to that observed previously by our research group for the uranyl β-ketoiminate complex, $UO_2(^{Ar}acnac)_2$.[22,23] Most importantly, the observation that the stronger U=O bonds of $UO_2(dbm)_2(THF)$, relative to $UO_2(^{Ar}acnac)_2$, are also susceptible to reductive silylation suggests that the scope of this transformation is broader than originally thought.

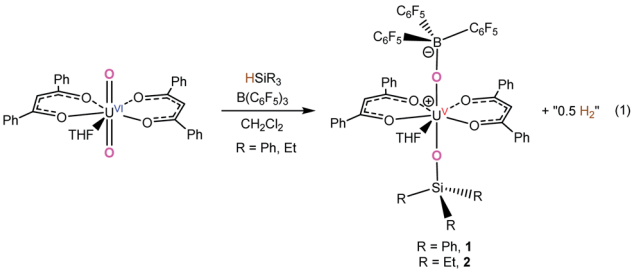

Complexes **1** and **2** both crystallize in the triclinic space group P-1 as a hexane solvate, $\mathbf{1}\cdot C_6H_{14}$, and a toluene and hexane solvate, $\mathbf{2}\cdot C_7H_8\cdot 0.5C_6H_{14}$, respectively. The solid-state molecular structure of **2** is shown in Fig. 1. Both **1** and **2** exhibit pentagonal bipyramidal geometries, as determined from the inter-ligand bond angles. For instance, complex **1** exhibits an

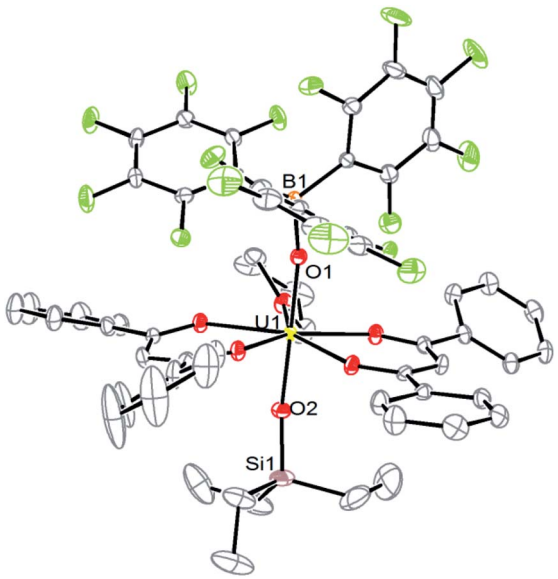

Fig. 1 Solid-state molecular structure of U(OB{C_6F_5}$_3$)(OSiEt$_3$)(dbm)$_2$(THF)$\cdot C_7H_8\cdot 0.5C_6H_{14}$ (**2**$\cdot C_7H_8\cdot 0.5C_6H_{14}$) with 50% probability ellipsoids. Solvate molecules and hydrogen atoms have been omitted for clarity.

O_B–U–O_{Si} bond angle of 175.06(8)°, while the O_{eq}–U–O_{ax} bond angles range from 84.06(8) to 95.42(8)°.[52–54] In both complexes, one uranyl oxo ligand has been converted to a silyloxide group, while the other oxo ligand is coordinated to a molecule of $B(C_6F_5)_3$, as was observed for $U(OB\{C_6F_5\}_3)(OSiPh_3)(^{Ar}acnac)_2$.[22] For complex **1**, the U–O_{Si} and U–O_B bond lengths are 2.024(2) and 1.9521(19) Å, respectively, while for **2**, they are 2.011(2) and 1.9600(19) Å, respectively (Table 1). These values are comparable to those previously reported for U(v)-silyloxide and U(v)-$OB(C_6F_5)_3$ distances,[13,15,22,23] and are indicative of a substantial reduction of the U=O bond order. Interestingly, the U–O_{dbm} bond lengths in **1** (av. U–O = 2.281 Å) and **2** (av. U–O = 2.282 Å) (Table 1) are shorter than those observed in other uranyl dbm complexes (*ca.* 2.35 Å).[55] Finally, both **1** and **2** feature a THF molecule coordinated to the uranium center. This contrasts with the reductive silylation product of $UO_2(^{Ar}acnac)_2$, for which no coordinated solvent is observed, a consequence of the reduced steric profile of the dbm ligand *vs.* the much bulkier ^{Ar}acnac ligand.

The ^{1}H NMR spectrum of **1** in CD_2Cl_2 consists of four broad resonances at 10.76, 4.75, 4.54, and 3.60 ppm in a 4 : 4 : 2 : 1 ratio, respectively, which correspond to the four proton environments of the dbm ligand. Additionally, three sharper resonances are observed at 7.53, 7.41, and 6.22 ppm in a 2 : 1 : 2 ratio, which correspond to the *m*-, *p*-, and *o*-proton environments of the Ph_3Si group. Similarly, the ^{1}H NMR spectrum of **2** in CD_2Cl_2 consists of four broad resonances at 7.40, 6.66, 6.26 and 4.54 ppm in a 2 : 4 : 4 : 1 ratio, respectively, as well as two broad resonances at 4.94 and 3.48 ppm, which correspond to the two Et_3Si proton environments. The $^{19}F\{^1H\}$ NMR spectrum of **1** consists of three resonances at −136.21, −160.49, and −165.75 ppm, in a 2 : 1 : 2 ratio, corresponding to the *o*-, *p*-, and *m*-fluorine atoms of the C_6F_5 groups. Similarly, the $^{19}F\{^1H\}$ NMR spectrum of **2** consists of three resonances at −135.00, −160.69, and −165.86 ppm, in a 2 : 1 : 2 ratio. Finally, the near-IR spectra for **1** and **2** are similar to those of other U(v) complexes (see Fig. S29 and S30†),[10,15,22,23] supporting the presence of a $5f^1$ ion.

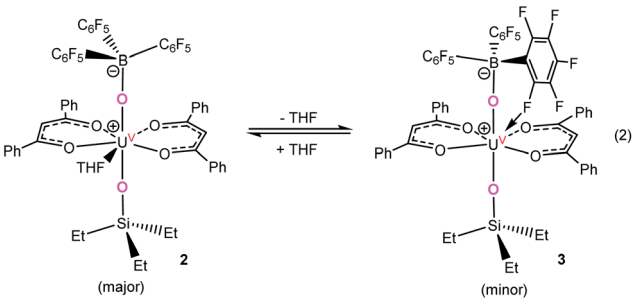

Interestingly, crystallization of **2** without the addition of 0.25 equiv. of THF to the supernatant led to the isolation of a second, minor product, $U(\kappa^2\text{-}O,F\text{-}OB\{C_6F_5\}_3)(OSiEt_3)(dbm)_2$ (**3**), as red-orange crystals in low yield (eqn (2)). Complex **3** could not be completely separated from complex **2** and so could not be fully characterized. Nonetheless, we were able to perform a single crystal X-ray diffraction study on this molecule. Complex **3** crystallizes in the triclinic space group $P\bar{1}$ and its solid-state molecular structure is shown in Fig. 2. The U–O_{Si} and U–O_B bond lengths of **3**, 1.981(3) and 1.915(2) Å, respectively, are comparable to those observed in complexes **1** and **2**. In contrast, the U–O–B bond angle (151.6(2)°) in **3** is considerably smaller than those observed in **1** (172.03(16)°) and **2** (165.80(18)°), likely due to the presence of a F → U dative interaction between an *o*-fluorine atom of the $B(C_6F_5)_3$ moiety and the uranium centre, which occurs in place of ligation of the THF solvate molecule. Interestingly, F → M dative interactions in uranium organometallics are quite rare and to our knowledge have only been observed in four other complexes. $[Cp^*_2Co][U\{OB(C_6F_5)_3\}_2(^{Ar}acnac)(OEt_2)]$[10] exhibits two F → U dative interactions, while $U^{IV}(NPh^F_2)_4$ ($Ph^F = C_6F_5$), $U^{IV}(NPhPh^F)_4$, and $U^{III}(NPh^F_2)_3(THF)_2$ exhibit three or more F → U interactions each.[56] The U–F distance for complex **3** (2.654(2) Å) falls on the shorter end of U–F dative interactions, which range from ∼2.60–2.93 Å.[10,56]

The $^{19}F\{^1H\}$ NMR spectrum of **3** consists of two resonances at −160.20 and −165.53 ppm in a 1 : 2 ratio, which are assignable to the *p*- and *m*-fluorine atoms of the C_6F_5 groups. In addition, a

Table 1 Selected bond lengths (Å) and angles (deg) for complexes **1–4**

	1	**2**	**3**	**4**[a]
U–O_{Si}	2.024(2)	2.011(2)	1.981(3)	
U–O_B	1.9521(19)	1.9600(19)	1.915(2)	1.958(18), 1.933(18), *1.920*
U–$O_{dbm\text{-}cis}$	2.2458(18)	2.2496(19)	2.235(3)	2.228(16), 2.188(14), *2.233*
	2.2795(19)	2.2583(19)	2.252(3)	2.238(13), 2.274(16), *2.270*
	2.280(2)	2.3014(19)	2.257(3)	2.255(16), 2.276(15), *2.263*
	2.317(2)	2.320(2)	2.277(3)	2.295(14), 2.279(13), *2.286*
				2.37(2), 2.27(2), *2.317*
U–$O_{dbm\text{-}trans}$				2.144(18), 2.250(18), *2.211*
U–F			2.654(2)	
O–Si	1.665(2)	1.681(2)	1.720(3)	
O–B	1.525(4)	1.503(4)	1.546(5)	1.52(4), 1.50(4)
O_{Si}–U–O_B	175.06(8)	178.43(8)	169.31(11)	
U–O–Si	164.04(13)	153.52(13)	148.7(2)	
U–O–B	172.03(16)	165.80(18)	151.6(2)	159.9(19), 160.9(19), *164.3*

[a] Two independent molecules in the asymmetric unit. Calculated data in italics.

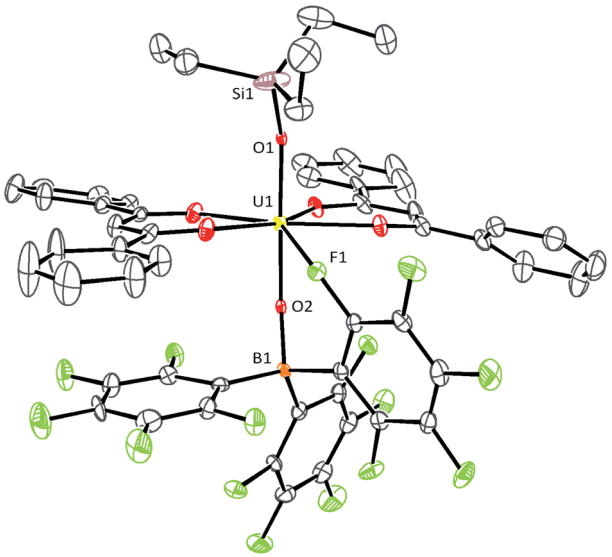

Fig. 2 Solid-state molecular structure of U(κ^2-*O,F*-OB{C_6F_5}$_3$)(OSiEt_3)(dbm)$_2$ (**3**) with 50% probability ellipsoids. Hydrogen atoms have been omitted for clarity.

very broad resonance assignable to the *o*-fluorine atoms is observed at −149.25 ppm. Notably, this resonance is shifted significantly upfield in comparison to those observed for **1** and **2**, suggestive of some interaction with the paramagnetic U(v) centre.[56] However, the observation of only a single peak for the *o*-fluorine atoms is indicative of free rotation about the B–C bond. Also present in the spectrum are resonances at 161.6 and 166.3 ppm, which are attributable to complex **2**. Interestingly, complexes **2** and **3** are also both observed in the *in situ* $^{19}F\{^1H\}$ NMR spectrum of the reaction between $UO_2(dbm)_2(THF)$, $HSiEt_3$, and $B(C_6F_5)_3$ (Fig. S9†). We suggest that complexes **2** and **3** are in equilibrium, and addition of THF to the mother liquor during crystallization favours the formation **2**, permitting its isolation in higher yields.

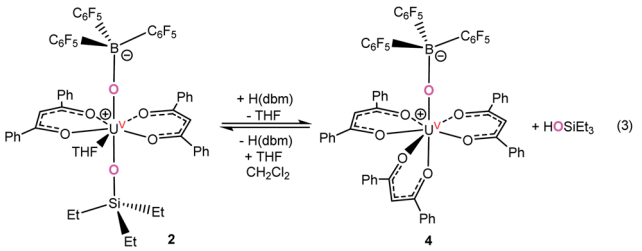

Given the rarity of well-defined oxo ligand substitution reactions for the uranyl moiety, we explored the ligand exchange reactivity of this new family of functionalized uranyl complexes. We hypothesized that the small steric profile of the equatorial dbm ligands would allow for facile axial ligand exchange. Gratifyingly, the addition of 1 equiv. of H(dbm) to **2** in CH_2Cl_2 results in the formation of U(OB{C_6F_5}$_3$)(dbm)$_3$ (**4**), which could be isolated as dark red crystalline material in 33% yield (eqn (3)). The isolation of complex **4** represents a rare example of controlled uranyl oxo ligand cleavage at ambient temperature and pressure.

Complex **4** crystallizes in the triclinic space group *P*1 as a toluene and hexane solvate, **4**·2C_7H_8·C_6H_{14}, with two independent molecules in the asymmetric unit. Its solid-state molecular structure is shown in Fig. 3. The uranium ion in complex **4** is coordinated by three dbm ligands and a $B(C_6F_5)_3$-capped oxo ligand. While the geometry about the uranium center in complex **4** can be described as a distorted pentagonal bipyramidal (CSM = 3.80), according to the continuous shape measure developed by Alvarez and co-workers,[57] it is probably better described as a distorted capped trigonal prism (CSM = 1.27), wherein the three dbm ligands define the trigonal prism and the O(B{C_6F_5}$_3$) ligand forms the capping group. The U–O_B bond lengths of the two independent molecules (1.96(2) and 1.93(2) Å, Table 1) are comparable to those observed for complexes **1**, **2**, and **3**, but longer than that observed for the U(v) mono-oxo complex, U(O)$(NR_2)_3$ (R = $SiMe_3$), which features a U–O bond length of 1.817(1) Å.[58] The elongated U–O bond in **4** is clearly the result of borane coordination to the oxo ligand. The U–O distances associated with the dbm oxygen atoms that are situated *trans* to the O(B{C_6F_5}$_3$) ligand are 2.14(2) and 2.25(2) Å, while the average U–$O_{dbm\text{-}cis}$ bond length is 2.27(4) Å.

Interestingly, the X-ray diffraction data for complex **4** are suggestive of the presence of the Inverse Trans Influence (ITI),[53,59–61] with the average *trans* U–O bond length being 0.07 Å shorter than the average *cis* bond (averaged over the two independent molecules in the asymmetric unit). However, it should be noted that the diffraction data for **4** are of modest quality, which leads to large uncertainties in the metrical parameters. We therefore turned to computational chemistry in the form of density functional theory to explore the possibility of an ITI in **4**. Initial geometry optimization using the GGA PBE functional suggested that, if the ITI is present, it is very small, with a *trans*

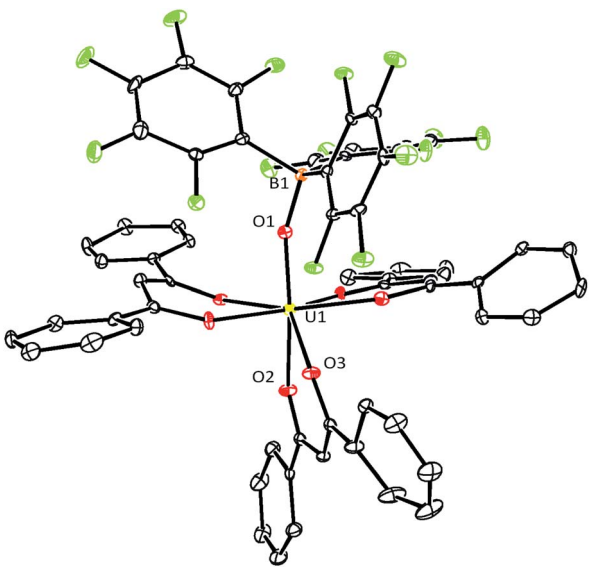

Fig. 3 Solid-state molecular structure of U(OB{C_6F_5}$_3$)(dbm)$_3$·2C_7H_8·C_6H_{14} (**4**·2C_7H_8·C_6H_{14}) with 50% probability ellipsoids. Complex **4** crystallizes with two independent molecules in the asymmetric unit; only one is pictured here. Solvate molecules and hydrogen atoms have been omitted for clarity.

shortening of only 0.018 Å. However, the overall agreement between theory and experiment, although adequate (mean absolute deviation (MAD) between the calculated and experimental U–O bond lengths of 0.021 Å), prompted us to re-optimize the geometry with the hybrid PBE0 functional. Agreement between theory and experiment is better at this level (MAD = 0.012 Å), and PBE0 also suggests a more pronounced ITI of 0.063 Å, much closer to the experimental value.

The ITI was first suggested by Denning in 1992 (ref. 62) in relation to oxy anions, such as $[UOCl_5]^-$. Experimentally, the ITI in this system is very pronounced, at 0.103 Å as determined by X-ray crystallography. For comparison, we have calculated the geometry of $[UOCl_5]^-$ at both the PBE and PBE0 levels, obtaining an ITI of 0.044 Å and 0.069 Å, respectively. It would therefore appear that PBE0 describes the ITI better than PBE in $[UOCl_5]^-$, providing justification for its use in calculating the geometry of complex **4**. One explanation for the ITI, first proposed by Denning[63,64] is that hybridization of the actinide 6p and 5f orbitals enhances σ bonding to the strongly bound trans directing ligand and leads to a partial hole in the 6p shell directed toward the trans ligand. This 6p hole enhances 5f overlap in the trans position, leading to a shortening of the trans bond. At the NPA/PBE0 level, we find the 6p populations of $[UOCl_5]^-$ and **4** to be 5.876 and 5.915, respectively, further supporting the suggestion of an ITI in complex **4**.

Starting from the fully optimized geometries of $[UOCl_5]^-$ and **4**, we have conducted relaxed potential energy surface scans of the bond trans to the oxo ligand, altering the trans bond length in steps of ±0.025 Å to a limit of ±0.1 Å from equilibrium. The results are shown in Fig. 4, and reveal that these potential surfaces are very flat. Compression (the steeper, left side of the well) of the trans bond in $[UOCl_5]^-$ by 0.1 Å raises the energy of the anion by only *ca.* 6 kJ mol^{-1}, and by less than 4 kJ mol^{-1} for **4**. It would therefore appear that the ITI is a rather subtle effect, even in prototypical systems such as $[UOCl_5]^-$. It is also interesting to note that for complex **4**, the energetic gain on moving from a structure where the *cis* and *trans* distances are about the same (*i.e.*, no ITI) to the fully optimised structure is about 1 kJ mol^{-1}. This is much smaller than the 6 kcal mol^{-1} stabilization afforded by the ITI in $[((^{t\mathrm{Bu}}\mathrm{ArO})_3\mathrm{tacn})\mathrm{U(O)(OTf)}]$,[65] which likely reflects their different oxidation states and the coordination of $B(C_6F_5)_3$ to the oxo ligand in **4**.

The ^{1}H NMR spectrum of **4** in CD_2Cl_2 consists of four broad resonances at 8.22, 7.68, 6.70 and 6.24 ppm in a 1 : 2 : 4 : 4 ratio, which corresponds to the four dbm proton environments and indicates that there is only one dbm environment observed at room temperature. In addition, the $^{19}F\{^1H\}$ NMR spectrum of **4** consists of three resonances at −144.72, −160.57, and −165.98 ppm, in a 2 : 1 : 2 ratio, corresponding to the *o*-, *p*-, and *m*-fluorine atoms of the C_6F_5 groups. Finally, the near-IR spectrum for **4** is similar to those of other U(v) complexes,[10,15,22,23] supporting the presence of a $5f^1$ ion. DFT also supports this description of the electronic structure of complex **4**. The uranium spin density at the Mulliken and Hirshfeld levels is 1.12 and 1.06, respectively, and examination of the α and β spin valence molecular orbitals finds an α spin orbital, with 62% uranium 5f character (Mulliken analysis), which has no β spin equivalent (Fig. 5).

To determine the fate of the missing Et_3SiO– group upon formation of **4**, we monitored the reaction of **2** with 1 equiv. of H(dbm) by NMR spectroscopy. The *in situ* $^{19}F\{^1H\}$ NMR spectrum of the reaction mixture revealed the formation of complex **4**, as evidenced by a characteristic resonance at −144.8 ppm, along with the presence of complex **2**. Complexes **2** and **4** were observed in a 2.4 : 1 ratio, respectively, according to the integrations of their *o*-fluorine resonances (Fig. S18†). More importantly, the *in situ* $^{13}C\{^1H\}$ NMR spectrum of the reaction mixture reveals the formation of $HOSiEt_3$, as evidenced by resonances at 6.21 and 5.56 ppm (Fig. S17†).[66] The proposed reaction stoichiometry was further confirmed by following the reaction of **4** with 1 equiv. of $HOSiEt_3$, and 1 equiv. of THF, in CD_2Cl_2 by ^{1}H and $^{19}F\{^1H\}$ NMR spectroscopies, which reveals the formation of complex **2** and H(dbm), along with complete consumption of complex **4** (Fig. S19 and S20†). This transformation represents a rare example of a controlled, reversible

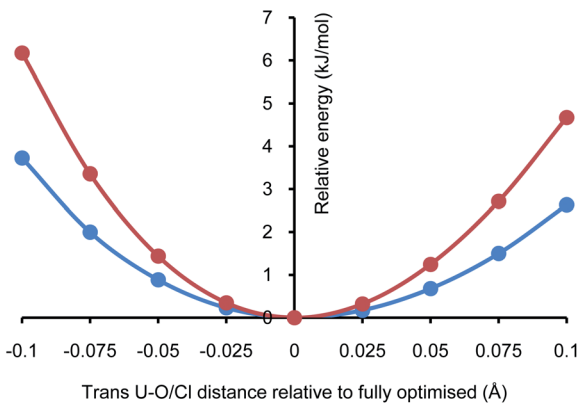

Fig. 4 Relaxed PBE0 potential energy surface scans of the trans bond in $[UOCl_5]^-$ (red) and **4** (blue).

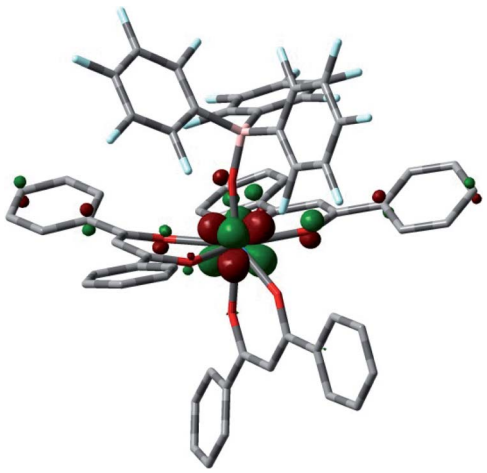

Fig. 5 Three dimensional representation of the uranium 5f-based α spin molecular orbital of **4**. Isosurface value = 0.05. Hydrogen atoms omitted for clarity.

uranyl U=O bond cleavage, in which the fate of the cleaved oxo ligand has been explicitly determined.[9,12,36,67,68] Reaction of **1** with 1 equiv. of H(dbm) in CD_2Cl_2 also results in formation of **4**, as determined by ^1H and $^{19}F\{^1H\}$ NMR spectroscopies. This experiment reveals the presence of complexes **1** and **4** in a 3 : 2 ratio, respectively. (Fig. S14 and S15†).

Conclusions

Reaction of $UO_2(dbm)_2(THF)$ with 1 equiv. of $HSiR_3$ (R = Ph, Et), in the presence of 1 equiv. of $B(C_6F_5)_3$, results in formation of $U(OB\{C_6F_5\}_3)(OSiR_3)(dbm)_2(THF)$ (R = Ph, **1**; Et, **2**) *via* oxo ligand silylation. The isolation of complexes **1** and **2** demonstrates that the borane-activated silylation of the uranyl oxo ligand does not require the highly donating β-ketoiminate ligand, ^{Ar}acnac, to proceed. Instead, oxo ligand silylation can be achieved with weaker donors attached to the uranyl equatorial sites. This work further demonstrates the generality of the borane-mediated reductive silylation protocol. Interestingly, reaction of **2** with 1 equiv. of H(dbm) results in formation of $U(OB\{C_6F_5\}_3)(dbm)_3$ (**4**), along with $HOSiEt_3$. We propose that this oxo ligand substitution chemistry is possible because of the narrow steric profile of the dbm ligand, which permits the coordination of the three dbm moieties to uranium, in addition to the borane-capped oxo ligand. Finally, complex **4** has been determined to show an inverse trans influence (ITI), based on comparison of diffraction and density functional theory data. The potential well for distorting the trans U–O from its equilibrium position is found computationally to be very flat, suggesting that the ITI is a subtle effect. For future studies, we plan to explore whether borane-activated silylation can proceed with cationic uranyl complexes, as the oxo ligands in these species are anticipated to be substantially less nucleophilic than those in a neutral molecule.

Experimental section

General

All reactions and subsequent manipulations were performed under anaerobic and anhydrous conditions under an atmosphere of nitrogen. Hexanes, diethyl ether, and toluene were dried using a Vacuum Atmospheres DRI-SOLV solvent purification system, and stored over 3 Å molecular sieves for 24 h prior to use. CH_2Cl_2 and CD_2Cl_2 were dried over activated 3 Å molecular sieves for 24 h before use. THF was distilled twice, first from calcium hydride and then from sodium benzophenone ketyl, and stored over 3 Å molecular sieves for 24 h prior to use. $UO_2Cl_2(THF)_3$ was synthesized by the published procedure.[69] $UO_2(dbm)_2(THF)$ was synthesized by modifying the previously reported procedure for the preparation of $UO_2(hfac)_2(THF)$ (see below).[49,70,71] All other reagents were purchased from commercial suppliers and used as received.

NMR spectra were recorded on a Varian UNITY INOVA 400 MHz spectrometer or a Varian UNITY INOVA 500 MHz spectrometer. ^1H and $^{13}C\{^1H\}$ NMR spectra are referenced to external $SiMe_4$ using the residual protio solvent peaks as internal standards (^1H NMR experiments) or the characteristic resonances of the solvent nuclei (^{13}C NMR experiments). $^{19}F\{^1H\}$ NMR spectra were referenced to external $CFCl_3$ in C_6D_6. Raman and IR spectra were recorded on a Mattson Genesis FTIR/Raman spectrometer with a NXR FT Raman Module. IR samples were recorded as KBr pellets, while Raman samples were recorded in an NMR tube as neat solids. UV-vis/NIR experiments were performed on a UV-3600 Shimadzu spectrophotometer. Elemental analyses were performed by the Microanalytical Laboratory at UC Berkeley.

Cyclic voltammetry measurements

CV experiments were performed with a CH Instruments 600c Potentiostat, and the data were processed using CHI software (version 6.29). All experiments were performed in a glove box using a 20 mL glass vial as the cell. The working electrode consisted of a platinum disk embedded in glass (2 mm diameter), the counter electrode was a platinum wire, and the reference electrode consisted of AgCl plated on Ag wire. Solutions employed during CV studies were typically 1 mM in the metal complex and 0.1 M in $[Bu_4N][PF_6]$. All potentials are reported *versus* the $[Cp_2Fe]^{0/+}$ couple. For all trials, $i_{p,a}/i_{p,c} = 1$ for the $[Cp_2Fe]^{0/+}$ couple, while $i_{p,c}$ increased linearly with the square root of the scan rate (*i.e.*, $\sqrt{v}$).

$UO_2(dbm)_2(THF)$

To a stirring THF (3 mL) solution of $UO_2Cl_2(THF)_3$ (435.2 mg, 0.781 mmol) was added dropwise a solution of H(dbm) (343.4 mg, 1.545 mmol) and $NaN(SiMe_3)_2$ (291.4 mg, 1.587 mmol) in THF (3 mL). This resulted in formation of a light orange solution. This solution was stirred for 24 h, whereupon the solution was filtered through a Celite column supported on glass wool (0.5 cm × 2 cm) to remove NaCl. The solution was then concentrated *in vacuo*, layered with hexanes (3 mL), and stored at −25 °C for 24 h, which resulted in the deposition of an orange powder. The solid was then extracted into dichloromethane (6 mL), and filtered through a Celite column supported on glass wool (0.5 cm × 2 cm). The filtrate was then concentrated *in vacuo*, layered with hexanes (3 mL), and stored at −25 °C for 24 h, which resulted in the deposition of an orange powder (440.2 mg, 71% yield). Anal. calcd $UO_7C_{34}H_{30}$: C, 51.78; H, 3.83; N, 0.00. Found: C, 51.55; H, 3.45; N, <0.2. ^1H NMR (CD_2Cl_2, 25 °C, 400 MHz): δ 8.50 (br s, 8H, ortho C*H*), 7.66 (br s, 8H, meta C*H*), 7.64 (br s, 4H, para C*H*), 7.32 (br s, 2H, γ-C*H*), 4.99 (br s, 4H, THF), 2.47 (br s, 4H, THF). $^{13}C\{^1H\}$ NMR (CD_2Cl_2, 25 °C, 126 MHz): δ 189.03 (s, *C*=O), 140.37 (s, ipso *C*), 132.88 (s, para *C*H), 129.46 (s, ortho *C*H), 128.98 (s, meta *C*H), 98.59 (s, γ-*C*H), 74.76 (s, THF), 27.43 (s, THF). IR (KBr pellet, cm^{-1}): 1597(sh w), 1591(m), 1549(sh m), 1535(vs), 1520(vs), 1477(m), 1452(m), 1440(w), 1360(s), 1348(m), 1313(m), 1298(m), 1224(sh w), 1221(w), 1180(w), 1159(w), 1122(w), 1067(w), 1022(sh w), 1024(w), 939(w), 906(s), 873(w), 840(w), 785(w), 750(m), 717(m), 684(m), 617(w), 604(w), 519(m). Raman (cm^{-1}): 3061(w), 1595(s), 1522(w), 1514(w), 1491(m), 1444(w), 1333(sh w), 1317(s), 1290(s), 1225(w), 1182(w), 1155(w), 1063(w), 1001(m), 939(w), 823(m, U=O ν_{sym}), 685(w), 561(w).

$U(OB\{C_6F_5\}_3)(OSiPh_3)(dbm)_2(THF)$ (1)

To a stirring orange dichloromethane (3 mL) solution of $UO_2(dbm)_2(THF)$ (143.3 mg, 0.181 mmol) was added dropwise a solution of Ph_3SiH (47.3 mg, 0.182 mmol) and $B(C_6F_5)_3$ (91.9 mg, 0.179 mmol) in dichloromethane (2 mL). This resulted in the immediate formation of a dark red solution. This solution was stirred for 15 h, whereupon the deep red solution was filtered through a Celite column supported on glass wool (0.5 cm × 2 cm). The solution was then concentrated *in vacuo*, THF (4 μL, 0.049 mmol) was added, and the solution was layered with hexanes (2 mL) and stored at −25 °C for 24 h, which resulted in the deposition of brown-red crystals (184.8 mg, 62% yield). Anal. calcd $UO_7SiBF_{15}C_{70}H_{45}$: C, 53.89; H, 2.91. Found: C, 53.62; H, 3.02. ^{1}H NMR (CD_2Cl_2, 25 °C, 400 MHz): δ 10.76 (br s, 8H, dbm CH), 7.53 (s, 6H, Ph_3Si meta CH), 7.41, (t, $J_{HH} = 5.6$ Hz, 3H, Ph_3Si para CH), 6.22 (s, 6H, Ph_3Si ortho CH), 4.75 (br s, 8H, dbm CH), 4.54 (br s, 4H, dbm para CH), 3.60 (br s, 2H, γ-CH), −1.21(br s, 4H, THF), −1.96 (br s, 4H, THF). ^{19}F{^{1}H} NMR: (CD_2Cl_2, 25 °C, 376 MHz): δ −136.24 (br s, 6F, ortho CF), −160.50 (s, 3F, para CF), −165.76 (s, 6F, meta CF). UV-vis/NIR (CH_2Cl_2, 3.85 × 10^{-3} M, L mol^{-1} cm^{-1}): 894 (ε = 12), 1114 (ε = 17), 1146 (sh, ε = 12), 1300 (sh, ε = 9), 1362 (ε = 19), 1438 (sh, ε = 12), 1462 (sh, ε = 11), 1606 (ε = 75). IR (KBr pellet, cm^{-1}): 1643(w), 1595(sh w), 1589(m), 1518(*vs.*), 1486(sh m), 1479(m), 1466(s), 1441(m), 1429(w), 1381(vw), 1373(vw), 1340(m), 1317(m), 1296(m), 1280(m), 1225(w), 1180(vw), 1157(vw), 1117(m), 1093(m), 1068(w), 1022(w), 993(sh vw), 978(m), 941(w), 875(sh w), 847(m), 820(s), 814(sh m), 787(w), 768(sh w), 764(w), 742(w), 714(w), 698(w), 683(w), 671(sh w), 617(w), 601(w), 574(vw), 528(m), 511(m), 461(sh m), 445(sh m), 418(sh vs), 414(vs), 407(vs).

$U(OB\{C_6F_5\}_3)(OSiEt_3)(dbm)_2(THF)$ (2)

To a stirring orange dichloromethane (3 mL) solution of $UO_2(dbm)_2(THF)$ (127.0 mg, 0.160 mmol) was added dropwise a solution of Et_3SiH (26 μL, 0.162 mmol) and $B(C_6F_5)_3$ (81.9 mg, 0.160 mmol) in dichloromethane (2 mL), which resulted in the immediate formation of a dark red solution. The solution was stirred for 24 h, whereupon the deep red solution was filtered through a Celite column supported on glass wool (0.5 cm × 2 cm). The solution was then concentrated *in vacuo*. THF (4 μL, 0.049 mmol) was added, and the solution was layered with hexanes (2 mL) and stored at −25 °C for 24 h, which resulted in the deposition of red-orange crystals (126.1 mg, 55% yield). Anal. calcd $UO_7SiBF_{15}C_{58}H_{45}$: C, 49.20; H, 3.20. Found: C, 49.24; H, 3.36. ^{1}H NMR (CD_2Cl_2, 25 °C, 400 MHz): δ 7.40 (t, $J_{HH} = 6.0$ Hz, 4H, para CH), 6.66 (br s, 8H, ortho CH), 6.26 (s, 8H, meta CH), 4.94 (br s, 6H, CH_2CH_3), 4.54 (br s, 2H, γ-CH), 3.48 (br s, 9H, CH_2CH_3), −1.10 (br s, 4H, THF), −2.03 (br s, 4H, THF). ^{19}F{^{1}H} NMR (CD_2Cl_2, 25 °C, 376 MHz): δ −135.00 (br s, 6F, ortho CF), −160.69 (t, J_{FF} = 13.9 Hz, 3F, para CF), −165.86 (d, J_{FF} = 16.2 Hz, 6F, meta CF). UV-vis/NIR (CH_2Cl_2, 4.15 × 10^{-3} M, L mol^{-1} cm^{-1}): 878 (ε = 11), 1118 (ε = 17), 1334 (ε = 18), 1438 (sh, ε = 12), 1420 (sh, ε = 7), 1608 (ε = 103). IR (KBr pellet, cm^{-1}): 1643(w), 1595(sh w), 1589(w), 1525(vs), 1518(sh vs), 1489(m), 1481(m), 1466(s), 1441(m), 1342(m), 1317(m), 1296(w), 1281(w), 1227(w), 115(sh w), 1094(m), 1068(w), 1022(w), 978(m), 941(w), 820(m), 810(m), 766(sh w), 760(w), 746(w), 717(w), 685(w), 669(sh w), 601(w), 527(w).

$U(OB\{C_6F_5\}_3)(OSiEt_3)(dbm)_2$ (3)

To a stirring orange dichloromethane (3 mL) solution of $UO_2(dbm)_2(THF)$ (264.6 mg, 0.335 mmol) was added dropwise a solution of Et_3SiH (100 μL, 0.626 mmol) and $B(C_6F_5)_3$ (171.6 mg, 0.335 mmol) in dichloromethane (2 mL), which resulted in formation of a dark red solution. The solution was stirred for 24 h, whereupon the deep red solution was filtered through a Celite column supported on glass wool (0.5 cm × 2 cm). The solvent was removed *in vacuo*, which resulted in formation of a dark red oil. The oil was triturated with Et_2O (2 × 4 mL), and then extracted into dichloromethane (4 mL). The solution was then concentrated *in vacuo* and layered with hexanes (2 mL). Storage at −25 °C for 24 h produced a dark red oil, which was discarded. The supernatant was further concentrated and layered with more hexanes (2 mL). Storage at −25 °C for another 24 h resulted in the deposition of a red-orange crystalline solid (106.5 mg, 24% yield). ^{1}H NMR (CD_2Cl_2, 25 °C, 400 MHz): δ 7.45 (br s, 4H, para CH), 6.45 (br s, 8H, meta CH), 6.00 (br s, 8H, ortho CH), 5.24 (br s, 6H, CH_2CH_3), 2.93 (br s, 9H, CH_2CH_3). The γ-C*H* resonance was not identified. ^{19}F{^{1}H} NMR (CD_2Cl_2, 25 °C, 376 MHz): δ −149.25 (br s, 6F, ortho CF), −160.20 (br t, J_{FF} = 11 Hz, 3F, para CF), −165.53 (d, J_{FF} = 18 Hz, 6F, meta CF).

$U(OB\{C_6F_5\}_3)(dbm)_3$ (4)

To a stirring dark red-orange dichloromethane solution (3 mL) of **2** (92.6 mg, 0.065 mmol) was added dropwise a dichloromethane (1 mL) solution of dibenzoylmethane (16.5 mg, 0.073 mmol). The solution was stirred for 1 h, whereupon the solution was filtered through a Celite column supported on glass wool (0.5 cm × 2 cm). The solution was then concentrated *in vacuo*, layered with hexanes (2 mL), and stored at −25 °C for 24 h, which resulted in the deposition of a dark red solid (18.5 mg, 33% yield). X-ray quality crystals were grown out of toluene solution layered with hexanes. Anal. calcd $UO_7BF_{15}C_{63}H_{33}$: C, 52.70; H, 2.32. Found: C, 52.65; H, 1.97. ^{1}H NMR (CD_2Cl_2, 25 °C, 400 MHz): δ 8.24 (br s, 3H, γ-CH), 7.68 (t, 6H, para CH), 6.71 (d, 12H, ortho CH), 6.22 (br s, 12H, meta CH). ^{19}F{^{1}H} NMR (CD_2Cl_2, 25 °C, 376 MHz): δ −144.79 (br s, 6F, ortho CF), −160.54 (t, J_{FF} = 19.7 Hz, 3F, para CF), −166.01 (d, J_{FF} = 19.9 Hz, 6F, meta CF). UV-vis/NIR (CH_2Cl_2, 2.75 × 10^{-3} M, L mol^{-1} cm^{-1}): 714 (sh, ε = 30), 950 (ε = 27), 1128 (sh, ε = 12), 1164 (sh, ε = 27), 1202 (ε = 36), 1482 (ε = 108), 1904 (ε = 34). IR (KBr pellet, cm^{-1}): 1643(w), 1591(sh m), 1587(m), 1522(sh vs), 1514(vs), 1487(sh m), 1470(s), 1466(s), 1437(m), 1371(w), 1340(sh w), 1317(m), 1294(m), 1280(m), 1225(w), 1184(w), 1109(sh w), 1095(m), 1067(m), 1024(w), 974(m), 939(w), 870(w), 831(w), 768(sh w), 758(w), 721(sh w), 717(w), 685(m), 602(w), 532(w), 523(sh w).

X-ray crystallography

The solid-state molecular structures of complexes **1–4** were determined similarly with exceptions noted in the following

paragraph. Crystals were mounted on a cryoloop under Paratone-N oil. Data collection was carried out on a Bruker KAPPA APEX II diffractometer equipped with an APEX II CCD detector using a TRIUMPH monochromator with a Mo Kα X-ray source ($\alpha = 0.71073$ Å). Data for **1**, **2**, and **4** were collected at 100(2) K, while data for **3** were collected at 150(2) K, using an Oxford nitrogen gas cryostream system. A hemisphere of data was collected using ω scans with 0.3° frame widths. Frame exposures of 5, 10, 10 and 10 seconds were used for complexes **1**, **2**, **3**, and **4** respectively. Data collection and cell parameter determination were conducted using the SMART program.[72] Integration of the data frames and final cell parameter refinement were performed using SAINT software.[73] Absorption correction of the data was carried out empirically based on reflection ψ-scans using the multi-scan method SADABS.[74] Subsequent calculations were carried out using SHELXTL.[75] Structure determination was done using direct or Patterson methods and difference Fourier techniques. All hydrogen atom positions were idealized, and rode on the atom of attachment. Structure solution, refinement, graphics, and creation of publication materials were performed using SHELXTL.[75]

Complex **2** exhibits positional disorder of the toluene solvent molecule. The positional disorder was addressed by modeling the molecule in two orientations, in a 50 : 50 ratio. The EADP, DFIX, and FLAT commands were used to constrain both orientations of the toluene molecule. For complex **4**, every non-hydrogen atom in one of the uranium molecule was constrained using the EADP command to its symmetry equivalent atom on the other uranium molecule. Two toluene solvent molecules were not refined anisotropically. In addition, the C–C bonds of the toluene rings were constrained with the DFIX command, while the rings were constrained with the FLAT command. Hydrogen atoms were not assigned to disordered carbon atoms. A summary of relevant crystallographic data for **1–4** is presented in Table S2.†

Computational details

Density functional theory calculations were carried out using the PBE[76,77] and PBE0 functionals[78] as implemented in the Gaussian 09 Rev. C.01 (ref. 79) quantum chemistry code. A (14s 13p 10d 8f)/[10s 9p 5d 4f] segmented valence basis set with Stuttgart–Bonn variety relativistic effective core potential was used for U. Dunning's cc pVTZ basis sets were employed for oxygen and boron, while other atoms were treated at the cc-pVDZ level. The ultrafine integration grid was employed, as were the default geometry and SCF convergence criteria. Natural population analyses were performed using the GenNBO6 code,[80] using 0.47 files from G09 as input.

Acknowledgements

This work was supported by the U.S. Department of Energy, Office of Basic Energy Sciences, Chemical Sciences, Biosciences, and Geosciences Division under Contract no. DE-FG02-09ER16067. N. K. thanks University College London for computing resources *via* the Research Computing "Legion" cluster (Legion@UCL) and associated services. E. A. P. thanks the NSF PIRE-ECCI program for a fellowship.

Notes and references

1 W.-M. Wu, J. Carley, M. Fienen, T. Mehlhorn, K. Lowe, J. Nyman, J. Luo, M. E. Gentile, R. Rajan, D. Wagner, R. F. Hickey, B. Gu, D. Watson, O. A. Cirpka, P. K. Kitanidis, P. M. Jardine and C. S. Criddle, *Environ. Sci. Technol.*, 2006, **40**, 3978–3985.
2 W.-M. Wu, J. Carley, T. Gentry, M. A. Ginder-Vogel, M. Fienen, T. Mehlhorn, H. Yan, S. Caroll, M. N. Pace, J. Nyman, J. Luo, M. E. Gentile, M. W. Fields, R. F. Hickey, B. Gu, D. Watson, O. A. Cirpka, J. Zhou, S. Fendorf, P. K. Kitanidis, P. M. Jardine and C. S. Criddle, *Environ. Sci. Technol.*, 2006, **40**, 3986–3995.
3 J. C. Renshaw, L. J. C. Butchins, F. R. Livens, I. May, J. M. Charnock and J. R. Lloyd, *Environ. Sci. Technol.*, 2005, **39**, 5657–5660.
4 B. Gu, W.-M. Wu, M. A. Ginder-Vogel, H. Yan, M. W. Fields, J. Zhou, S. Fendorf, C. S. Criddle and P. M. Jardine, *Environ. Sci. Technol.*, 2005, **39**, 4841–4847.
5 E. S. Ilton, A. Haiduc, C. L. Cahill and A. R. Felmy, *Inorg. Chem.*, 2005, **44**, 2986–2988.
6 N. Kaltsoyannis and P. Scott, *The f elements*, Oxford University Press, New York, 1999.
7 R. G. Denning, *J. Phys. Chem. A*, 2007, **111**, 4125–4143.
8 S. Fortier and T. W. Hayton, *Coord. Chem. Rev.*, 2010, **254**, 197–214.
9 M. P. Wilkerson, C. J. Burns, H. J. Dewey, J. M. Martin, D. E. Morris, R. T. Paine and B. L. Scott, *Inorg. Chem.*, 2000, **39**, 5277–5285.
10 D. D. Schnaars, G. Wu and T. W. Hayton, *J. Am. Chem. Soc.*, 2009, **131**, 17532–17533.
11 M. J. Sarsfield and M. Helliwell, *J. Am. Chem. Soc.*, 2004, **126**, 1036–1037.
12 K. W. Bagnall and J. G. H. du Preez, *Chem. Commun.*, 1973, 820–821.
13 P. L. Arnold, D. Patel, C. Wilson and J. B. Love, *Nature*, 2008, **451**, 315–318.
14 P. L. Arnold, J. B. Love and D. Patel, *Coord. Chem. Rev.*, 2009, **253**, 1973–1978.
15 J. L. Brown, G. Wu and T. W. Hayton, *J. Am. Chem. Soc.*, 2010, **132**, 7248–7249.
16 Q.-J. Pan, S. O. Odoh, G. Schreckenbach, P. L. Arnold and J. B. Love, *Dalton Trans.*, 2012, **41**, 8878–8885.
17 G. M. Jones, P. L. Arnold and J. B. Love, *Angew. Chem., Int. Ed.*, 2012, **51**, 12584–12587.
18 P. L. Arnold, G. M. Jones, S. O. Odoh, G. Schreckenbach, N. Magnani and J. B. Love, *Nat. Chem.*, 2012, **4**, 221–227.
19 G. M. Jones, P. L. Arnold and J. B. Love, *Chem.–Eur. J.*, 2013, **19**, 10287–10294.
20 A. Yahia, P. L. Arnold, J. B. Love and L. Maron, *Chem. Commun.*, 2009, 2402–2404.
21 A. Yahia, P. L. Arnold, J. B. Love and L. Maron, *Chem.–Eur. J.*, 2010, **16**, 4881–4888.

22 D. D. Schnaars, G. Wu and T. W. Hayton, *Inorg. Chem.*, 2011, **50**, 4695–4697.
23 D. D. Schnaars, G. Wu and T. W. Hayton, *Inorg. Chem.*, 2011, **50**, 9642–9649.
24 D. L. Clark, S. D. Conradson, R. J. Donohoe, D. W. Keogh, D. E. Morris, P. D. Palmer, R. D. Rogers and C. D. Tait, *Inorg. Chem.*, 1999, **38**, 1456–1466.
25 S. P. McGlynn, J. K. Smith and W. C. Neely, *J. Chem. Phys.*, 1961, **35**, 105–116.
26 P. G. Allen, J. J. Bucher, D. L. Clark, N. M. Edelstein, S. A. Ekberg, J. W. Gohdes, E. A. Hudson, N. Kaltsoyannis, W. W. Lukens, M. P. Neu, P. D. Palmer, T. Reich, D. K. Shuh, C. D. Tait and B. D. Zwick, *Inorg. Chem.*, 1995, **34**, 4797–4807.
27 K. I. M. Ingram, L. J. L. Haller and N. Kaltsoyannis, *Dalton Trans.*, 2006, 2403–2414.
28 P. L. Arnold, A.-F. Pécharman and J. B. Love, *Angew. Chem., Int. Ed.*, 2011, **50**, 9456–9458.
29 P. L. Arnold, E. Hollis, G. S. Nichol, J. B. Love, J.-C. Griveau, R. Caciuffo, N. Magnani, L. Maron, L. Castro, A. Yahia, S. O. Odoh and G. Schreckenbach, *J. Am. Chem. Soc.*, 2013, **135**, 3841–3854.
30 P. L. Arnold, E. Hollis, F. J. White, N. Magnani, R. Caciuffo and J. B. Love, *Angew. Chem., Int. Ed.*, 2011, **50**, 887–890.
31 G. Nocton, P. Horeglad, V. Vetere, J. Pecaut, L. Dubois, P. Maldivi, N. M. Edelstein and M. Mazzanti, *J. Am. Chem. Soc.*, 2010, **132**, 495–508.
32 G. Nocton, P. Horeglad, J. Pecaut and M. Mazzanti, *J. Am. Chem. Soc.*, 2008, **130**, 16633–16645.
33 V. Mougel, B. Biswas, J. Pecaut and M. Mazzanti, *Chem. Commun.*, 2010, **46**, 8648–8650.
34 L. Natrajan, F. Burdet, J. Pecaut and M. Mazzanti, *J. Am. Chem. Soc.*, 2006, **128**, 7152–7153.
35 V. Mougel, J. Pecaut and M. Mazzanti, *Chem. Commun.*, 2012, **48**, 868–870.
36 J.-C. Berthet, G. Siffredi, P. Thuéry and M. Ephritikhine, *Eur. J. Inorg. Chem.*, 2007, 4017–4020.
37 Y. Gong, V. Vallet, M. del Carmen Michelini, D. Rios and J. K. Gibson, *J. Phys. Chem. A*, 2014, **118**, 325–330.
38 D. J. Parks and W. E. Piers, *J. Am. Chem. Soc.*, 1996, **118**, 9440–9441.
39 D. J. Parks, J. M. Blackwell and W. E. Piers, *J. Org. Chem.*, 2000, **65**, 3090–3098.
40 J. M. Blackwell, E. R. Sonmor, T. Scoccitti and W. E. Piers, *Org. Lett.*, 2000, **2**, 3921–3923.
41 J. M. Blackwell, D. J. Morrison and W. E. Piers, *Tetrahedron*, 2002, **58**, 8247–8254.
42 J. M. Blackwell, K. L. Foster, V. H. Beck and W. E. Piers, *J. Org. Chem.*, 1999, **64**, 4887–4892.
43 A. Berkefeld, W. E. Piers and M. Parvez, *J. Am. Chem. Soc.*, 2010, **132**, 10660–10661.
44 K. M. Abubacker and N. S. K. Prasad, *J. Inorg. Nucl. Chem.*, 1961, **16**, 296–307.
45 K. Mizuguchi, S.-H. Lee, Y. Ikeda and H. Tomiyasu, *J. Alloys Compd.*, 1998, **271–273**, 163–167.
46 S.-Y. Kim, H. Tomiyasu and Y. Ikeda, *J. Nucl. Sci. Technol.*, 2002, **39**, 160–165.
47 T. Yayamura, S. Iwata, S.-i. Iwamaru and H. Tomiyasu, *J. Chem. Soc., Faraday Trans.*, 1994, **90**, 3253–3259.
48 L. Sacconi and G. Giannoni, *J. Chem. Soc.*, 1954, 2368–2372.
49 A. A. Tahir, M. Hamid, M. Mazhar, M. Zeller and A. D. Hunter, *Acta Crystallogr., Sect. E: Struct. Rep. Online*, 2006, **62**, m1780–m1781.
50 T. W. Hayton and G. Wu, *Inorg. Chem.*, 2009, **48**, 3065–3072.
51 J. L. Brown, C. C. Mokhtarzadeh, J. M. Lever, G. Wu and T. W. Hayton, *Inorg. Chem.*, 2011, **50**, 5105–5112.
52 D. Wester and G. J. Palenik, *J. Am. Chem. Soc.*, 1973, **95**, 6505–6506.
53 H. S. La Pierre and K. Meyer, *Inorg. Chem.*, 2013, **52**, 529–539.
54 J. Jiang, M. J. Sarsfield, J. C. Renshaw, F. R. Livens, D. Collison, J. M. Charnock, M. Helliwell and H. Eccles, *Inorg. Chem.*, 2002, **41**, 2799–2806.
55 S. Kannan, M. R. A. Pillai, V. Venugopal, P. A. Droege and C. L. Barnes, *Inorg. Chim. Acta*, 1997, **254**, 113–117.
56 H. Yin, A. J. Lewis, U. J. Williams, P. J. Carroll and E. J. Schelter, *Chem. Sci.*, 2013, **4**, 798–805.
57 D. Casanova, P. Alemany, J. M. Bofill and S. Alvarez, *Chem.–Eur. J.*, 2003, **9**, 1281–1295.
58 S. Fortier, J. L. Brown, N. Kaltsoyannis, G. Wu and T. W. Hayton, *Inorg. Chem.*, 2012, **51**, 1625–1633.
59 A. Kovács and R. J. M. Konings, *ChemPhysChem*, 2006, **7**, 455–462.
60 O. P. Lam, S. M. Franke, H. Nakai, F. W. Heinemann, W. Hieringer and K. Meyer, *Inorg. Chem.*, 2012, **51**, 6190–6199.
61 A. J. Lewis, P. J. Carroll and E. J. Schelter, *J. Am. Chem. Soc.*, 2013, **135**, 511–518.
62 R. Denning, *Struct. Bonding*, 1992, **79**, 215–276.
63 J. M. Bartleet, R. G. Denning and I. D. Morrison, *Mol. Phys.*, 1992, **75**, 601–612.
64 E. O'Grady and N. Kaltsoyannis, *Dalton Trans.*, 2002, 1233–1239.
65 B. Kosog, H. S. La Pierre, F. W. Heinemann, S. T. Liddle and K. Meyer, *J. Am. Chem. Soc.*, 2012, **134**, 5284–5289.
66 B. P. S. Chauhan, A. Sarkar, M. Chauhan and A. Roka, *Appl. Organomet. Chem.*, 2009, **23**, 385–390.
67 A. C. Bean, T. A. Sullens, W. Runde and T. E. Albrecht-Schmitt, *Inorg. Chem.*, 2003, **42**, 2628–2633.
68 J.-C. Berthet, P. Thuéry and M. Ephritikhine, *Chem. Commun.*, 2005, 3415–3417.
69 M. P. Wilkerson, C. J. Burns, R. T. Paine and B. L. Scott, *Inorg. Chem.*, 1999, **38**, 4156–4158.
70 G. M. Kramer, M. B. Dines, R. B. Hall, A. Kaldor, A. J. Jacobson and J. C. Scanlon, *Inorg. Chem.*, 1980, **19**, 1340–1347.
71 M. Alagar, K. Rajagopal, R. V. Krishnakumar, M. Subha Nandhini, S. Kannan and S. Natarajan, *Acta Crystallogr., Sect. E: Struct. Rep. Online*, 2003, **59**, m524–m526.
72 *SMART Apex II, Version 2.1*, Bruker AXS Inc., Madison, WI, 2005.
73 *SAINT Software User's Guide, Version 7.34a* Bruker AXS Inc. Madison, WI, 2005.
74 G. M. Sheldrick, *SADABS*, University of Gottingen, Germany, 2005.

75 *SHELXTL PC, Version 6.12*, Bruker AXS Inc., Madison, WI, 2005.
76 J. P. Perdew, K. Burke and M. Ernzerhof, *Phys. Rev. Lett.*, 1997, **78**, 1396.
77 J. P. Perdew, K. Burke and M. Ernzerhof, *Phys. Rev. Lett.*, 1996, **77**, 3865–3868.
78 C. Adamo and V. Barone, *J. Chem. Phys.*, 1999, **110**, 6158–6159.
79 M. J. Frisch, G. W. Trucks, H. B. Schlegel, G. E. Scuseria, M. A. Robb, J. R. Cheeseman, G. Scalmani, V. Barone, B. Mennucci, G. A. Petersson, H. Nakatsuji, M. Caricato, X. Li, H. P. Hratchian, A. F. Izmaylov, J. Bloino, G. Zheng, J. L. Sonnenberg, M. Hada, M. Ehara, K. Toyota, R. Fukuda, J. Hasegawa, M. Ishida, T. Nakajima, Y. Honda, O. Kitao, H. Nakai, T. Vreven, J. A. Montgomery, J. E. Peralta, F. Ogliaro, M. Bearpark, J. J. Heyd, E. Brothers, K. N. Kudin, V. N. Staroverov, R. Kobayashi, J. Normand, K. Raghavachari, A. Rendell, J. C. Burant, S. S. Iyengar, J. Tomasi, M. Cossi, N. Rega, J. M. Millam, M. Klene, J. E. Knox, J. B. Cross, V. Bakken, C. Adamo, J. Jaramillo, R. Gomperts, R. E. Stratmann, O. Yazyev, A. J. Austin, R. Cammi, C. Pomelli, J. W. Ochterski, R. L. Martin, K. Morokuma, V. G. Zakrzewski, G. A. Voth, P. Salvador, J. J. Dannenberg, S. Dapprich, A. D. Daniels, O. Farkas, J. B. Foresman, J. V. Ortiz, J. Cioslowski and D. J. Fox, *Gaussian 09, Revision C.01*, Gaussian, Inc. Wllington CT, 2009.
80 E. D. Glendening, J. K. Badenhoop, A. E. Reed, J. E. Carpenter, J. A. Bohmann, C. M. Morales, C. R. Landis and F. Weinhold, *NBO 6.0*, Theoretical Chemistry Institute, University of Wisconsin, Madison WI, 2013.